Pure Appl. Chem., Vol. 78, No. 10, pp. 1803–1822, 2006.
doi:10.1351/pac200678101803

Advancing conjugated polymers into nanometer-scale devices*

Wenping Hu[1,‡], Hiroshi Nakashima[2], Erjing Wang[1,3], Kazuaki Furukawa[2], Hongxiang Li[1], Yi Luo[4], Zhigang Shuai[1], Yoshiaki Kashimura[2], Yunqi Liu[1], and Keiichi Torimitsu[2]

[1]Beijing National Laboratory for Molecular Sciences, Laboratory of Organic Solids, Institute of Chemistry, Chinese Academy of Sciences, Beijing 100080, China; [2]NTT Basic Research Laboratories, NTT Corporation, 3-1 Morinosato Wakamiya, Atsugi, Kanagawa 243-0198, Japan; [3]Graduate School of Chinese Academy of Sciences, Beijing 100039, China; [4]Theoretical Chemistry, Royal Institute of Technology, AlbaNova, S-106 91 Stockholm, Sweden

Abstract: In this article, we review the possibility of combining conjugated polymers with nanometer-scale devices (nanodevices), in order to introduce the properties associated with conjugated polymers into such nanodevices. This approach envisages combining the highly topical disciplines of polymer electronics and nanoelectronics to engender a new subdirection of polymer nanoelectronics, which can serve as a tool to probe the behavior of polymer molecules at the nanometer/molecular level, and contribute to clarifying transport mechanisms in conjugated polymers. In this study, we exemplify this combination, using a family of linear and conjugated polymers, poly(*p*-phenylene-ethynylene)s (PPEs) with thiolacetate-functionalized end groups.

Keywords: polymers; nanometer-scale devices; nanodevices; conjugation; quantum.

INTRODUCTION

Since the discovery of conductive polymers in the 1970s, thousands of conjugated polymers have been synthesized and investigated, and some have been successfully applied in polymer electronics since the 1990s [1]. However, as far as we know, few reports have dealt with conjugated polymers at the nanometer level. Such investigations are expected to reveal the behavior of polymer molecules at the nanometer level, and thereby clarify transport mechanisms of polymer molecules, and also to facilitate the interpretation of certain biological phenomena. For example, there are no "chips" in the human brain, but the ability of biopolymers in brain tissue to transport and process complex information is incomparably superior to that of any chip. Moreover, the combination of polymers with nanometer-scale devices (nanodevices) offers scope to introduce the properties associated with conjugated polymers into such nanodevices. This field presently enjoys worldwide attention, and is undergoing rapid advancement in response to the promise that it offers for the next generation of electronic devices. Since conjugated polymers are cheaply available, and have special simple film forming ability (e.g., spin-coating) and excellent flexibility, they have great potential for applications in nanodevices.

---

*Paper based on a presentation at the 15th International Symposium on Fine Chemistry and Functional Polymers (FCFP-XV) and the 1st International Symposium on Novel Materials and their Synthesis (NMS-I), 17–20 October 2005, Shanghai, China. Other presentations are published in this issue, pp. 1803–1896.
‡Corresponding author

What kind of polymers are the possible candidates for nanodevices? A first prerequisite for the fabrication of nanodevices is to connect polymer molecules between electrodes, i.e., to wire polymer molecules into circuits. Therefore, there appear to be at least three essential requirements for polymer molecules to be wired: (i) conductivity (conductive polymers); (ii) rigidity (linear polymer backbone structure for wiring or bridging them between electrodes); and (iii) connectivity (the molecules could covalently attach to a metallic electrode for wiring). Many conjugated polymers meet the first basic requirement of conductivity, but lack the necessary rigidity and connectivity. For example, molecules of nonrigid polymers usually form dot or rope-like structures on substrates, e.g., polysilanes [2], which poses a challenge for wiring into an electrical circuit.

Amongst candidate polymers (oligomers are not included here), poly(*p*-phenylene-ethynylene)s (PPEs) seem to meet all the foregoing requirements. They are regarded as good electroluminescent materials and have been successfully applied in organic light-emitting devices [3]. The presence of the triple bond in PPE molecules prevents the rotation of adjacent phenyl rings with respect to each other, and thereby imposes the necessary rigidity. This property has been recognized by Müllen and Samorí, who have suggested the possibility of exploiting PPEs in nanotechnology (e.g., in nanowires) [4]. Furthermore, by modifying PPE with thiol/thioacetate-end-functionalized groups (so-called "molecular alligator clips" which can adhere to Au electrodes [5] via Au–S bonds), there are good prospects for connecting this thiol/thioacetate-end-functionalized polymer with Au electrodes.

Two approaches have been developed for wiring polymer molecules between electrodes. One employs an "SPM" (scanning tunneling microscopy, STM and conducting atomic force microscopy, AFM) tip to form tip/polymer/substrate devices [6,7], and the other employs mercury drop electrodes to form Hg/SAM/material/SAM/Hg devices [8]. We call these devices "prototype devices". Another technique uses nanogap electrodes (namely, a pair of electrodes with a nanometer gap [9–11]) to form metal/polymer/metal nanodevices. We call these "practical devices". "Prototype devices" are useful for basic research, e.g., Lindsay et al. have combined SPM and self-assembly techniques and obtained good results for molecular-level characterization [12]. Tao et al. further combined the SPM technique with a data statistical technique for molecular devices [13]. Although "prototype devices" have provided many important results, they are far from practical applications. Can we imagine a nanodevice that includes a huge SPM system? Furthermore, such devices are unrepresentative of the conditions under which they would be required (i.e., a high vacuum, no gate electrode, etc.). As a consequence, "practical devices" with nanogap electrodes have recently been attracting growing attention.

FABRICATING NANOGAP ELECTRODES FOR NANODEVICES

By using nanogap electrodes, even single molecular samples can be measured under which real devices operate. Many methods have already been employed for the fabrication of nanogap electrodes. These methods include vacuum evaporation [14], the breaking junction technique [15], electrochemical deposition (also called electroplating) [16], electron-beam lithography [17], electromigration [18], and the nanowire break method [19]. Successful examples have been reported for each of these methods. However, we found a way to fabricate nanogap electrodes by electroplating (electrodeposition) with high controllability, which requires no special technique or system. Nanogap electrodes can be fabricated with the desired gap width simply by monitoring and controlling the current flowing through the gap electrodes. Electrodes with a gap width of less than 1 nm have been obtained recently [16] by using this method.

Figure 1 shows the electroplating system. The initial electrodes for electroplating were fabricated by electron-beam lithography on a doped Si/SiO_2 (300 nm) substrate. The initial gap width of the electrodes was around 50–200 nm. The electrodes were installed on a stage with manual probes and placed in electroplating liquid in a small (2 mm diameter) Teflon tube, which acted as an electroplating bath. TEMPEREX 8400 (Tanaka Kikinzoku), including 1.17 % (w/w) $KAu(CN)_2$, was used as the electroplating liquid. A gold wire (0.5 mm diameter) was immersed in the solution as a counter electrode. A

bias voltage of 1.4–1.5 V was applied to the initial electrodes. With electroplating, we were able to fabricate nanogap electrodes with the desired gap width or with two or three fingers (see Fig. 2).

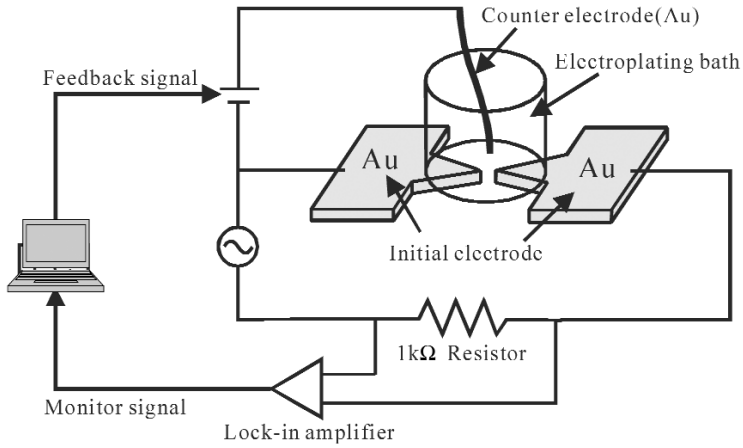

Fig. 1 Electroplating system used to fabricate nanogap electrodes with two gold fingers.

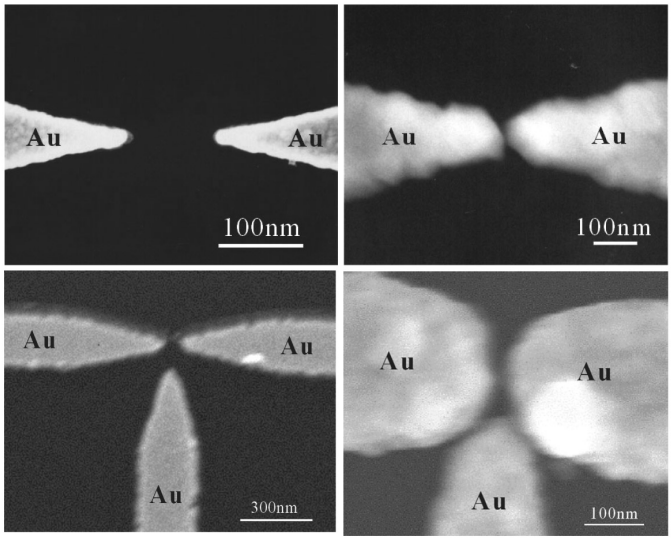

Fig. 2 SEM images of electrodes before and after electroplating. (Top) two-finger Au nanogap electrodes, (bottom) three-finger nanogap electrodes.

SYNTHESIS OF THIOACETATE-END-FUNCTIONALIZED PPE

As mentioned above, PPE with thiol/thioacetate-end-functionalized groups (TA-PPE) have the potential to be wired between Au nanogap electrodes. We demonstrated the fabrication of Au nanogap electrodes by electroplating. Here, we describe the synthesis of wired TA-PPE/TA-PPE molecules (Fig. 3).

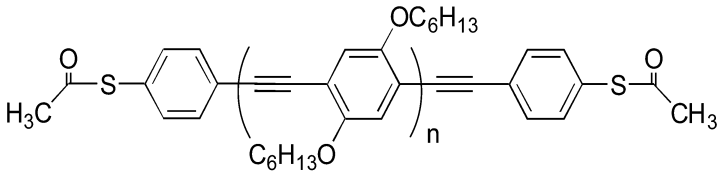

Fig. 3 Chemical structure of TA-PPE.

The synthesis of TA-PPE is described elsewhere [20] (M_w = 54 000, M_w/M_n = 2.47). Its UV–vis, fluorescence (FL) spectra, and FL anisotropy (FL-A) in dilute tetrahydrofuran (THF) solution are shown in Fig. 4. The UV–vis spectrum of TA-PPE exhibited an intense absorption band at 440 nm, and there was an FL emission at 480 nm, giving a Stokes shift of about 40 nm. In addition, the FL emission provided a highly efficient quantum yield (>0.5). The FL-A around the π–π* polymer backbone interband region had a high value of about 0.25~0.3, and was only weakly dependent on the photoexcitation wavelength. Theoretically, the FL-A value is defined from –0.2 (ω = 90 °) to 0.4 (ω = 0 °), where ω is the angle between the absorption moment and emission moment along the polymer backbone. The high FL-A value of PPE might thus support a linear and rigid-rod-type backbone conformation without kinks or folding.

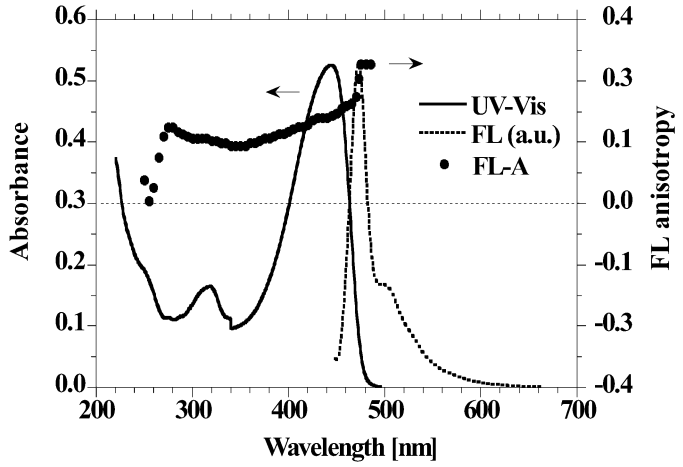

Fig. 4 UV–vis spectra, FL spectra (FL emission intensity normalized by UV–vis absorption intensity), and FL-A of PPE in dilute THF solution (ca. 1.71×10^{-5} mol/L) at room temperature.

CONDUCTIVITY OF TA-PPE

Conductive polymers were discovered in the 1970s, and the 2000 Nobel Prize in chemistry was awarded to Alan J. Heeger, Alan G. MacDiarmid, and Hideki Shirakawa "for the discovery and development of conductive polymers". PPE is a typical conductive polymer and is regarded as an electroluminescent material [3]. Therefore, there is no doubt about the conductivity of either PPE or TA-PPE. Here, we cite supplementary theoretical proof to emphasize this point. We used 24-unit TA-PPE as an example. Figure 5 shows the lowest unoccupied molecular orbital (LUMO) of the 24-unit TA-PPE. It is clear that all the electron clouds of the units overlap each other, which indicates the good conductivity of TA-PPE molecules.

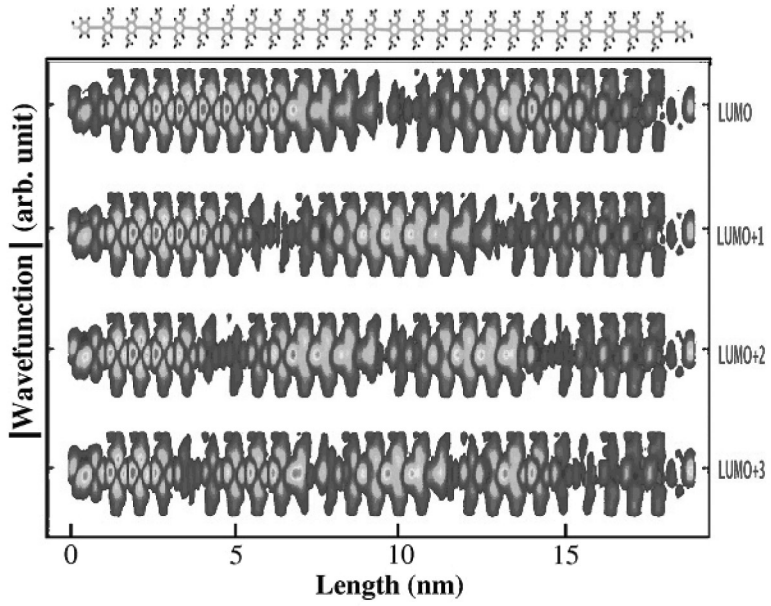

Fig. 5 Calculated LUMO of 24-unit TA-PPE molecule.

RIGIDITY OF TA-PPE

The rigidity of the TA-PPE molecules is a critical parameter as regards wiring them into circuits. Without rigidity, polymer molecules usually form dot and rope-like structures on substrates, e.g., polysilanes [2] (Fig. 6). However, our TA-PPE has a straight needle-like structure (Fig. 7) with an average length of 2–3 μm and a diameter of around ~200 nm. The straight, linear (rather than coiling) structure clearly suggests the rigidity of the polymer molecules.

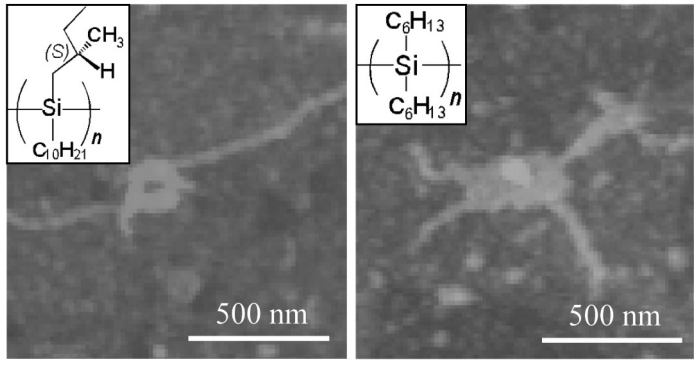

Fig. 6 Dot and rope-like structure of polysilanes formed on silicon substrates because of lack of molecular rigidity.

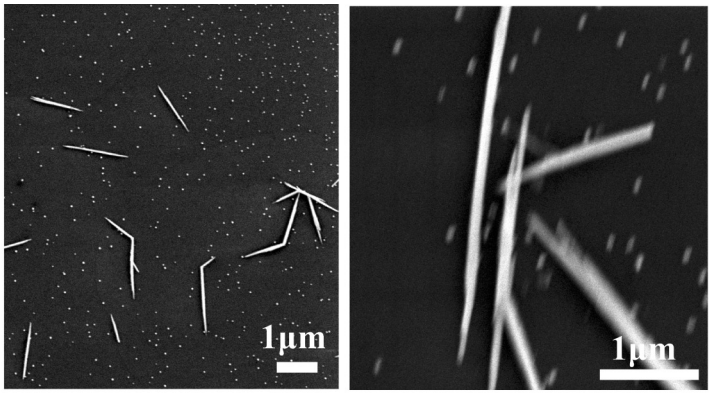

Fig. 7 SEM image of TA-PPE bundles on SiO_2 showing straight, linear needle-like structure.

It should be mentioned that the rigidity of TA-PPE molecules is a relative concept. We once tried to manipulate the needle-like structure with an AFM tip (Nanoman, DI Company), however, the needle-like TA-PPE structure was cut by the AFM tip instead of being moved [21]. Moreover, we found that small TA-PPE structures appear as straight nanowires (see Fig. 8, left) [22]. As its size increases, the TA-PPE takes the form of nanowires that can be bent (see Fig. 8, middle), and finally it appears as belt-like structures with excellent softness (see Fig. 8, right).

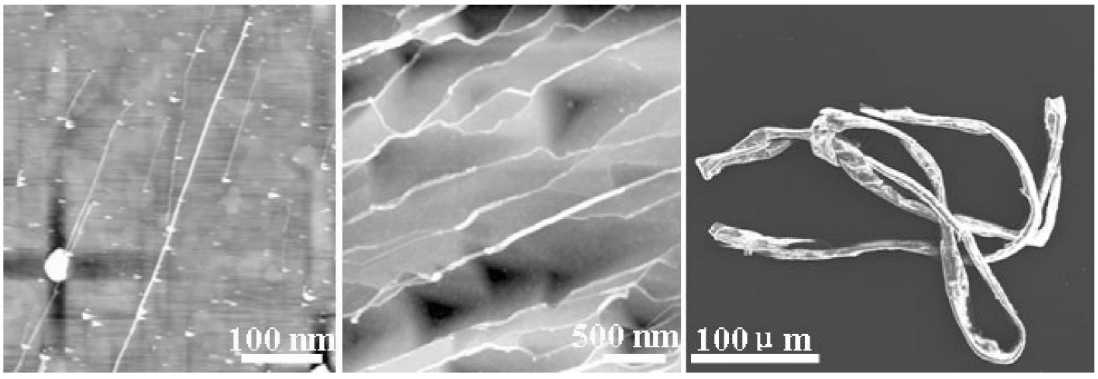

Fig. 8 Size dependence of rigidity of TA-PPE structure.

CONNECTIVITY OF TA-PPE

As regards TA-PPE connectivity, we began by using time-of-flight/secondary ion mass spectroscopy (TOF/SIMS) analysis (Physical Electronics Co., TRIFT III, Ga^+ ion source, acceleration voltage: 12 kV, analysis area: 100 μm^2) to observe chemisorbed TA-PPE on Au substrates. The results suggested that the sulfur ions on the substrate were present in greater quantities than the sulfur contamination in the air, and they were identified having masses of 109.02, 108.01, and 107.00. These values are consistent with the components of chemisorbed polymer end groups, namely $–S–C_6H_5$, $–S–C_6H_4$, and $–S–C_6H_3$ units, respectively. Furthermore, X-ray photoelectron spectroscopy (XPS) data (obtained with an ESCALab220i-XL electron spectrometer from VG Scientific using 300 W AlKα radiation) demonstrated the dominant S_{2p} resonance at 162.3 eV caused by the Au-bound thiolate (Fig. 9) [23].

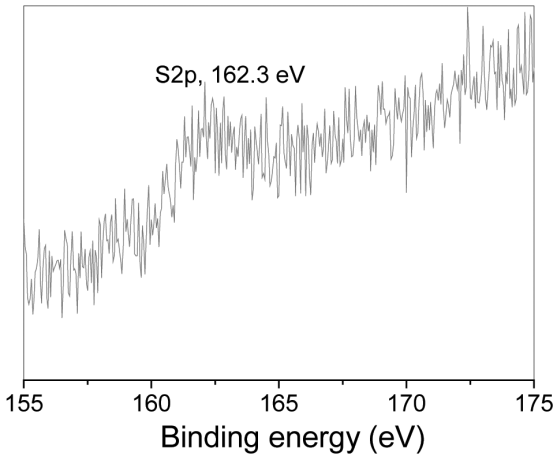

Fig. 9 S_{2p} peak of TA-PPE grafted on Au.

The UV–vis spectra of TA-PPE showed a clear absorption band only on Au/quartz substrates (Fig. 10) assigned to the π–π* transition of the PPE backbone. No absorption peaks were observed with Pt, ITO, or SiO_2 substrates, indicating that the selective chemisorption of TA-PPE coincided with the selectivity of solid surfaces. We could ignore the physical adsorption on the substrate surfaces from both the functionalized end groups and the side chains or conjugated main chain, because TA-PPE is easily removed from the Pt, ITO, and SiO_2 surfaces with our washing process, as supported by the absence of UV–vis peaks. This is probably due to the ineffective chemical affinity between the TA-PPE end group and the Pt, ITO, and SiO_2 substrate surfaces in contrast to its strong affinity with the Au surface. Moreover, when we mixed Au nanoparticles and TA-PPE in solution, we found that TA-PPE molecules are capable of capturing Au nanoparticles at both ends to form barbell-type molecules [24]. We confirmed and visualized the polymer connectivity at the end of the polymer from the effect of terminal functionalization.

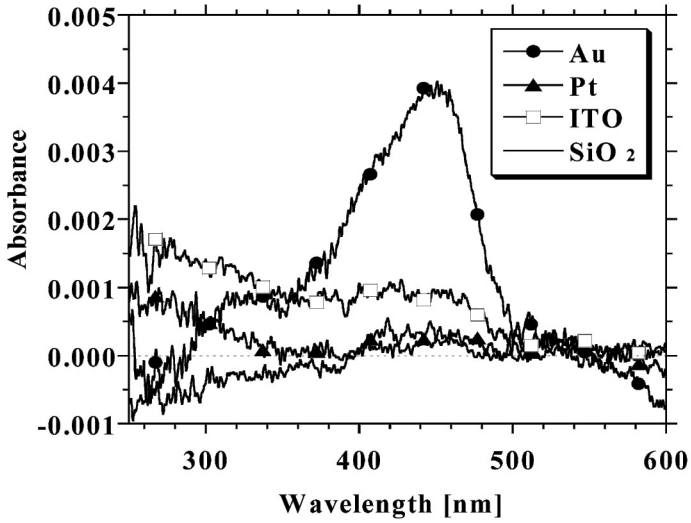

Fig. 10 UV–vis of TA-PPE on Au, Pt, ITO, or SiO_2 substrate surfaces at room temperature.

IN SITU WIRING OF TA-PPE MOLECULES BETWEEN NANOGAP ELECTRODES

It is clear that TA-PPE molecules meet the three basic requirements for wiring between nanogap electrodes: conductivity, rigidity, and connectivity. We therefore undertook the controlled wiring of TA-PPE molecules to investigate their photoelectric properties.

The wiring of TA-PPE molecules was monitored in situ with a highly sensitive current-time circuit (Fig. 11) in a metallic shielded chamber. As soon as one polymer molecule formed a successful connection between the Au nanogap electrodes, the nanojunction current jumped to a new value (Fig. 12). Scanning electron microscope (SEM) images of this type of self-assembled nanojunction have already been published [25] and are shown in Fig. 13. It is clear that the TA-PPE molecules were wired between the gap electrodes (gap width: ~40 nm). The diameter of the connected nanowire, estimated from its SEM image, was ~20 nm.

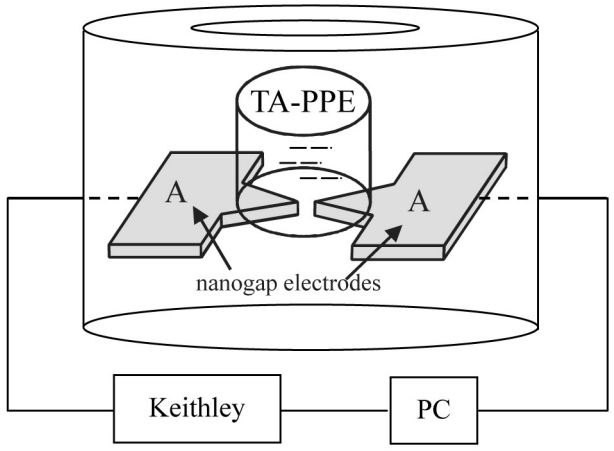

Fig. 11 In situ monitoring of wiring TA-PPE molecules between nanogap electrodes.

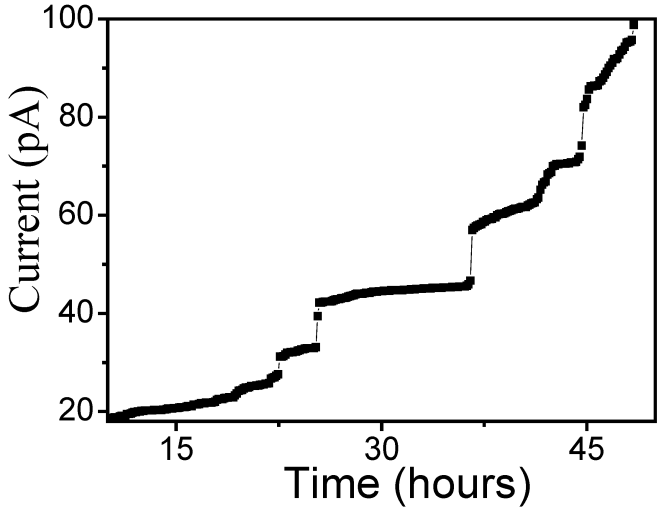

Fig. 12 Current-time curve of TA-PPE molecules wired between nanogap electrodes.

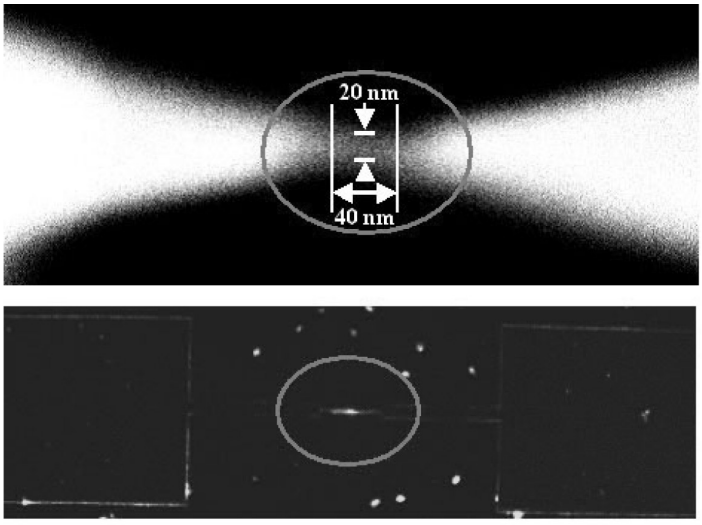

Fig. 13 SEM and fluorescent images of Au/TA-PPE/Au nanojunctions.

The current-voltage (I-V) characteristics (Fig. 14) of the connected nanojunctions exhibited two features [25]: (i) the current increases nonlinearly with increasing bias; and (ii) near-symmetrical I-V characteristics are realized with positive and negative applied bias, which indicates the symmetrical connection of the nanojunctions.

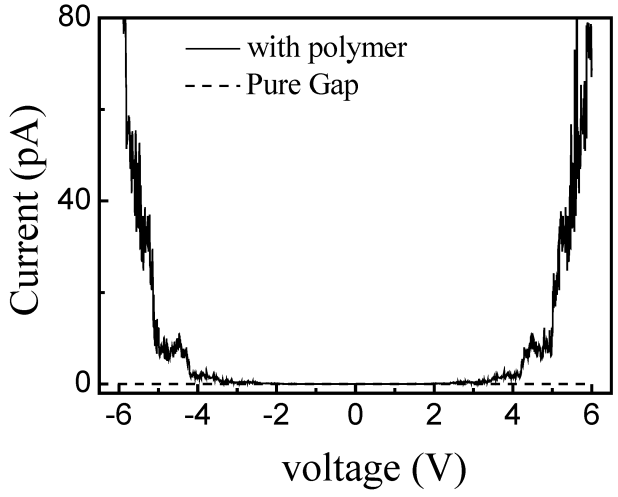

Fig. 14 I-V characteristics of Au/TA-PPE/Au self-assembled nanojunctions.

These steps are not the result of conductance quantization [26] because the step height is six orders of magnitude smaller than the conductance quantum, $2e^2/h$. Our nanojunctions exhibited no obvious temperature dependence in the 267–297 K range, which indicates that there is no thermal activation process in the carrier injection. Furthermore, when we analyzed the observed I-Vs in terms of thermal emission and space-charge-limited current models, they did not fit the dependence on voltage or temperature. These results indicate that the electrons are possibly caused by the tunneling mechanism. The geometry of the orbitals on the sulfurs of the TA-PPE molecules does not permit the conjugated π-or-

bitals from the polymer molecules to interact strongly with the conduction orbitals of the Au electrodes, and so the orbital mismatch creates a potential barrier at each connection interface between gap structure devices. It is highly possible that a self-assembled nanojunction is similar to a quantum dot junction, with the conjugated polymer molecules as a quantum dot and the terminal sulfur atoms acting as two tunnel barriers. Therefore, it is very important to clarify the carrier injection mechanism of the self-assembled TA-PPE nanojunctions (Fig. 15).

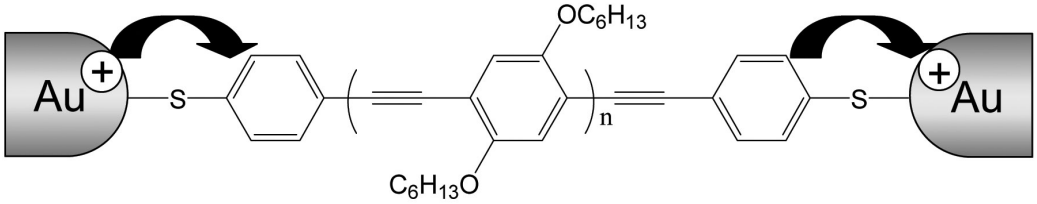

Fig. 15 Carrier injection model of Au/TA-PPE/Au self-assembled nanojunctions.

CARRIER INJECTION FROM Au ELECTRODE INTO TA-PPE

TA-PPE molecules have thioacetate-end-functionalized groups that can act as "molecular alligator clips" that make it possible to graft the molecules to the Au surface via Au–S bonds. Therefore, it is highly likely that carriers tunnel through the Au–S bond into the TA-PPE.

To confirm this, we fabricated two kinds of TA-PPE device with coplanar gap electrodes. The electrodes had a gap width of around 100 nm and were first cleaned successively with pure water, hot acetone, hot ammonia–hydrogen peroxide solution (ammonia:hydrogen oxide: water = 1:1:5), pure water, and pure ethanol. Then, several drops of TA-PPE (solvent: THF) were deposited around the electrode tip positions, and finally the electrodes were dried in a N_2 chamber. We selected THF as the solvent because TA-PPE has excellent solubility in THF, and THF can evaporate quickly due to its low boiling point. Because of the rapid volatilization of THF solvent in air, the TA-PPE molecules have insufficient time to rearrange themselves, which means that it is highly possible that TA-PPE retains its molecular arrangement as seen in the structure in Fig. 16a. We then placed the Fig. 16a sample in THF vapor again (in a bottle 1/3 filled with THF) for another 96 h treatment to give the TA-PPE molecules sufficient time to rearrange themselves at the Au/TA-PPE interface. Moreover, methods have been described whereby NH_4OH promotes the deprotection of acetate-protected thiols [5,27]. Therefore, 20 ml of ammonia solution was added to the THF solvents to activate the TA-PPE end groups for Au-TA-PPE connection. This treatment results in Au/TA-PPE interface as seen in Fig. 16b because of the fact that thiol/thioacetate-functionalized-end groups can graft themselves to Au surfaces. The I-V characteristics of the two kinds of devices were recorded with a BCT-21 MDC Probe Station (Nagase, Japan) and a Keithley 6430 in a vacuum chamber (2–3 Pa).

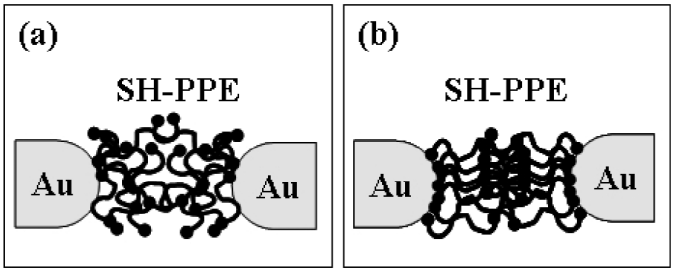

Fig. 16 (a) TA-PPE deposited between Au nanogap electrodes; (b) devices in (a) retreated in THF/ammonia vapor for 96 h.

The JVs in Fig. 16a exhibit two features: temperature dependence and some nonlinear I-V stepwise characteristics (Fig. 17). The temperature dependence suggests the existence of a thermal activation process during hole injection, and the nonlinear stepwise characteristics are probably due to the tunneling injection [28–30]. In fact, when we analyzed the data by using $\ln J \propto V^{1/2}$ or an Arrhenius plot (lnJ vs. 1/T), they did not fit either curve well. Therefore, it is probable that the hole injection is the result of a mixed mechanism in this case. After retreating the (a) devices for 96 h, the typical JVs (Fig. 18) of the treated samples exhibited the following characteristics [28]: (i) the current density is much larger than that of the untreated devices; (ii) the temperature dependence is unclear; and (iii) the nonlinear stepwise characteristics are clearer when the bias is changed. The improved current density suggested two possibilities: (i) improved hole injection (i.e., an improved interface between the TA-PPE and the Au electrodes) and (ii) a transformation of the bulk TA-PPE between the nanogap electrodes. However, when we changed the electrodes from Au to Pt (TA-PPE exhibits very weak adhesion to a Pt surface), before and after the same ammonia/THF treatment, the current densities of the device showed no obvious change. This indicated that the effect of ammonia/THF on bulk TA-PPE is not the key to the improved current density. That is, the improved current density is very likely to be due to the improved Au/TA-PPE interface. Moreover, the fact that there is no significant temperature dependence proved that there is a much weaker thermal activation process in the hole injection. An Arrhenius plot (lnJ vs. 1/T) of the (b) device shows no significant temperature dependence in the lnJ~1/T slope at different biases, which certainly reveals the absence of thermal activation in the sample after the ammonia/THF treatment. The above two points enabled us to conclude that the hole injection is now dominated by tunneling [28].

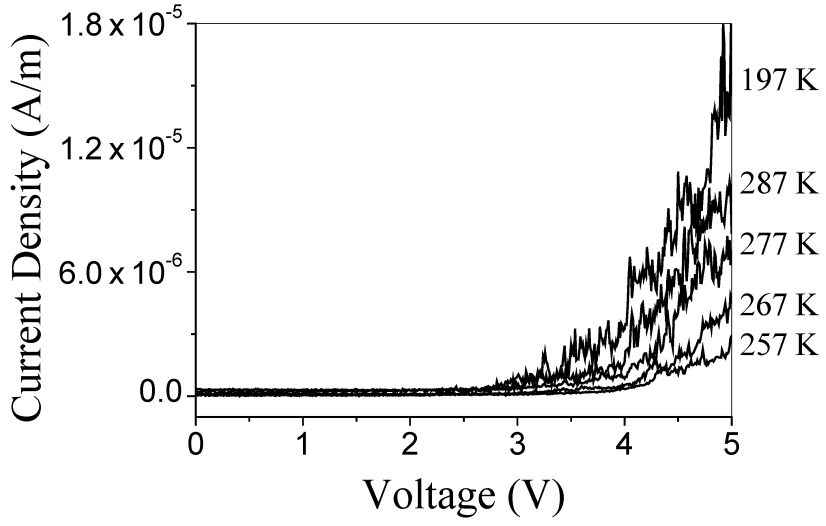

Fig. 17 I-V characteristics of Au/TA-PPE/Au gap device with new cast TA-PPE.

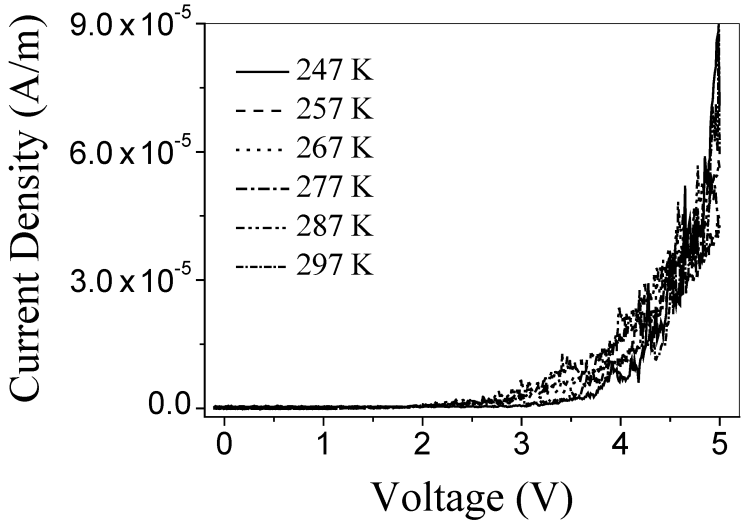

Fig. 18 I-V characteristics of Fig.17 device after being treated in ammonia/THF atmosphere for 96 h.

We assume that the carrier injection in Fig. 16b is "through Au–S bond" tunneling. Tunneling can be divided into direct tunneling (when $V \leq \Phi_B/e$) and Fowler–Nordheim tunneling (when $V \geq \Phi_B/e$). These two tunneling mechanisms can be distinguished by their voltage dependence as shown in the following equations [31,32]:

$$J \propto V \exp\left[-\frac{2w\sqrt{2m\Phi_B}}{\hbar}\right] \qquad \text{(direct tunneling at } V < \Phi_B/e\text{)}$$

$$J \propto V^2 \exp -\left[\frac{4w\sqrt{2m}}{3q\hbar V}(q\Phi_B)^{3/2}\right] \qquad \text{(Fowler–Nordheim tunneling at } V > \Phi_B/e\text{)}$$

Here, w is the gap width of the electrodes, m is the effective mass of the holes, $\hbar$ is Planck's constant, and Φ_B is the tunneling barrier height. We plot the results for devices shown in Fig. 15b with $\ln(J/V^2)$ vs. $1/V$ in Fig. 19. It is clear that all the curves can be divided into two parts. In a low bias range ($\frac{1}{V} > 0.75$), the curves of $\ln(J/V^2)$ vs. $1/V$ show no significant voltage dependence; in a high bias range ($\frac{1}{V} < 0.75$), the $\ln(J/V^2)$ vs. $1/V$ curves exhibit similar linear relationships. These results indicate that carrier injection is dominated by Fowler–Nordheim tunneling at a high bias and by direct tunneling at a low bias. The dividing point is around $1/V \approx 0.7$–0.75. Therefore, it is reasonable to deduce that the tunneling barrier height of the Au–S bond Φ_B is around 1.33–1.43 eV. The result agrees well with those of Reed et al. [32], who found that the Au–S tunneling barrier is around 1.39 ± 0.01 eV by studying the alkanethiol monolayer.

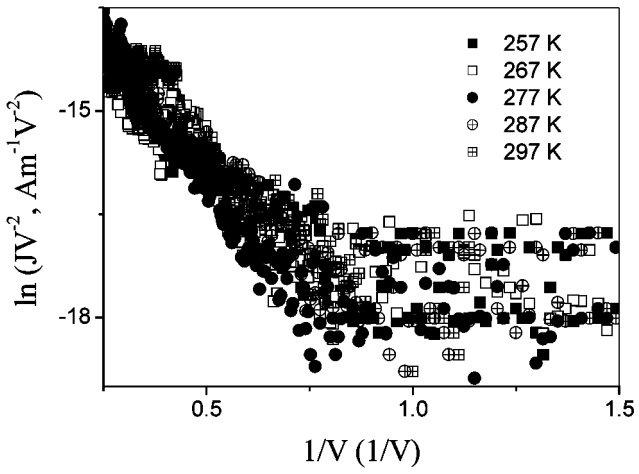

Fig. 19 $\ln JV^{-2}$ ~1/V relationship from results for (b) device.

SELF-ASSEMBLED NANOMETER-SCALE PHOTO SWITCHERS AND TRANSISTORS OF TA-PPE

The photo response behavior of the self-assembled Au/TA-PPE/Au nanojunction (gap width: 40 nm, TA-PPE nanowire connected between nanogap electrodes with a diameter of around 20 nm) under light irradiation exhibited two distinct states: (i) a "low" current state without irradiation and (ii) a "high" current state under illuminated conditions, worked as a nanometer-scale photo switcher [33]. The switching in these two states is fast and reversible. We observed a response velocity near 400 Hz in our experiments. In the "OFF" state, the resistance is as high as ~10^{15} Ω. In the "ON" state, the resistance is ~10^{12} Ω, the switching ratio is as high as 1000 (without polymer, under the same irradiation conditions there is a current change of only several tens of fA probably caused by the fact that the photons are trapped by the insulator layer: SiO_2).

As mentioned above, our self-assembled nanojunction very likely couples to electrodes with Au–S bonds at both ends, although the coupling strengths at the two ends are probably different. Without irradiation, when the applied bias is insufficiently high, the electrons and holes will be blocked by the tunneling barriers, therefore, the current is very low. With illumination, the photon-generated excitons will dissociate into free electrons and holes, and some possess sufficiently high energy to jump over or tunnel through the Au–S barrier, resulting in the high current ("on" state) of the tunneling junction.

The current of the tunneling junction exhibited a strong dependence on the intensity (Fig. 20) and wavelength (Fig. 21) of the incident light. The light intensity dependence is understandable because of the change in the photon density of the incident light. The wavelength dependence of the current response of the nanojunction exhibited an obvious red shift compared with the absorbance and excitation spectra of TA-PPE. The absorbance of TA-PPE is due to photon absorption and results in the direct promotion of an electron from its π to π* orbital, however, the current response of the photo switcher is based on the dissociation of the photon-generated excitons. Therefore, one explanation for the red shift of the current response is the exciton absorption of TA-PPE in the photo switcher.

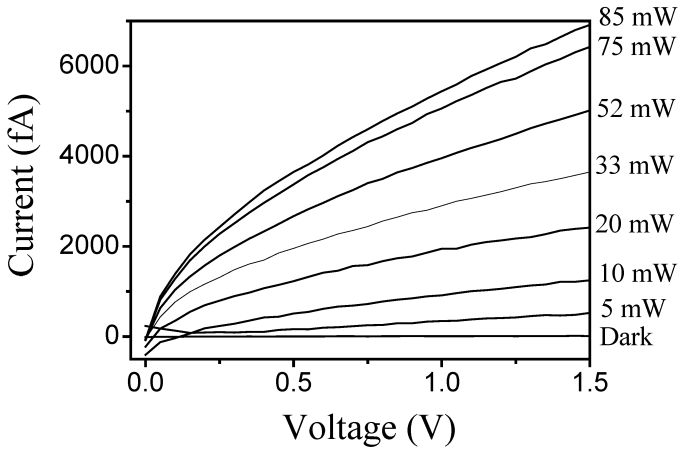

Fig. 20 Light intensity dependence of self-assembled nanojunctions.

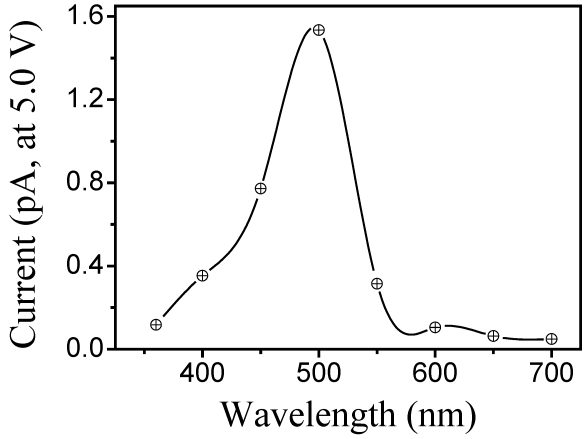

Fig. 21 Wavelength dependence of self-assembled nanojunctions.

In order to further clarify the electron transport through the optical switcher, we ohmicly connected the rear low-resistance Si substrate of the switcher as a gate electrode, and shifted the switcher into a nanometer-scale transistor. The output characteristics of the transistor suggest that the device works as a p-type transistor under an accumulated model (Fig. 22).

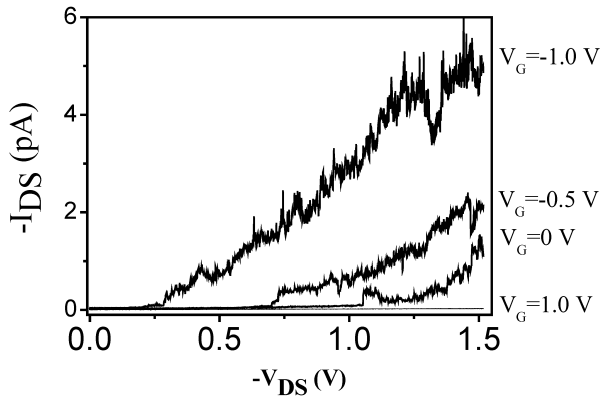

Fig. 22 Transistor behavior of self-assembled TA-PPE nanodevice.

When irradiated with light, the device exhibited better transistor behavior in the low operational voltage region (Fig. 23) because the photon-generated carriers formed conduction channel between the TA-PPE and the SiO_2 insulator, which suggested a possible way of obtaining photo-controlled devices (Fig. 24).

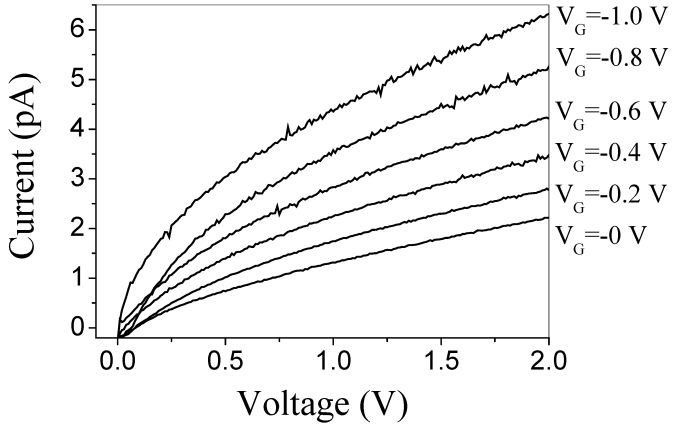

Fig. 23 Transistor behavior with light irradiation (white light, 85 mW).

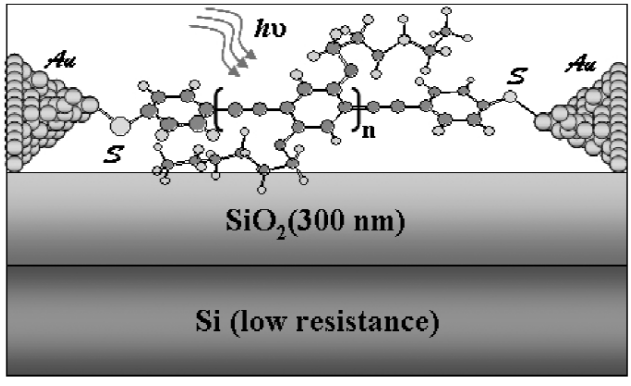

Fig. 24 Model of photo-controlled self-assembled TA-PPE nanodevices.

When we kept the drain voltage at 1.05 V to allow us to adjust the gate voltage continuously, the conductance at 147 K exhibited highly periodic oscillation with gate voltage, which appeared as a series of sharp and narrow peaks. All the peaks have an almost equidistant separation of ~40-50 mV. We assumed our self-assembled tunneling junction to be a quantum dot junction where the conjugated TA-PPE molecules form a dot, and with the terminal sulfur atoms acting as two tunnel barriers. Then, one interpretation of the highly periodic conductance is that it results from single-electron charging oscillations or Coulomb-blockade oscillations, which can be viewed as a manifestation of single-electron sequential tunneling through a system of two self-assembled tunnel junctions in series.

WIRING ONE OR SEVERAL TA-PPE MOLECULES INTO CIRCUIT

As mentioned above, the wiring of TA-PPE molecules between nanogap electrodes could be monitored in situ with a current-time circuit. We observed that as soon as one polymer molecule or one polymer bundle (several molecules) were trapped between the nanogap electrodes (i.e., a successful connection was formed between the nanogap electrodes), the current flow through the nanogap electrodes jumped to a new value. Therefore, we expected to obtain a molecular junction as soon as the first current jump was observed. At that point, we stopped the self-assembly process by gently removing the device from the polymer solution. To improve this procedure, the TA-PPE molecules were shortened to an average of 24 polymerization units (with a molecular length of around 18.3 nm) and the nanogap electrodes were electroplated with a gap width of around 18 nm so that they all matched [34]. After wiring one or several PPE molecules into the nanogap electrodes, we formed the Au/TA-PPE/Au molecular junction shown in Fig. 25. It should be stressed that the lack of a proper experimental tool with which to visualize the molecular junction made it difficult to identify the exact number of molecules between electrodes. The repeatability of the measurements at least allows us to believe that the molecules between the electrodes are always the same size.

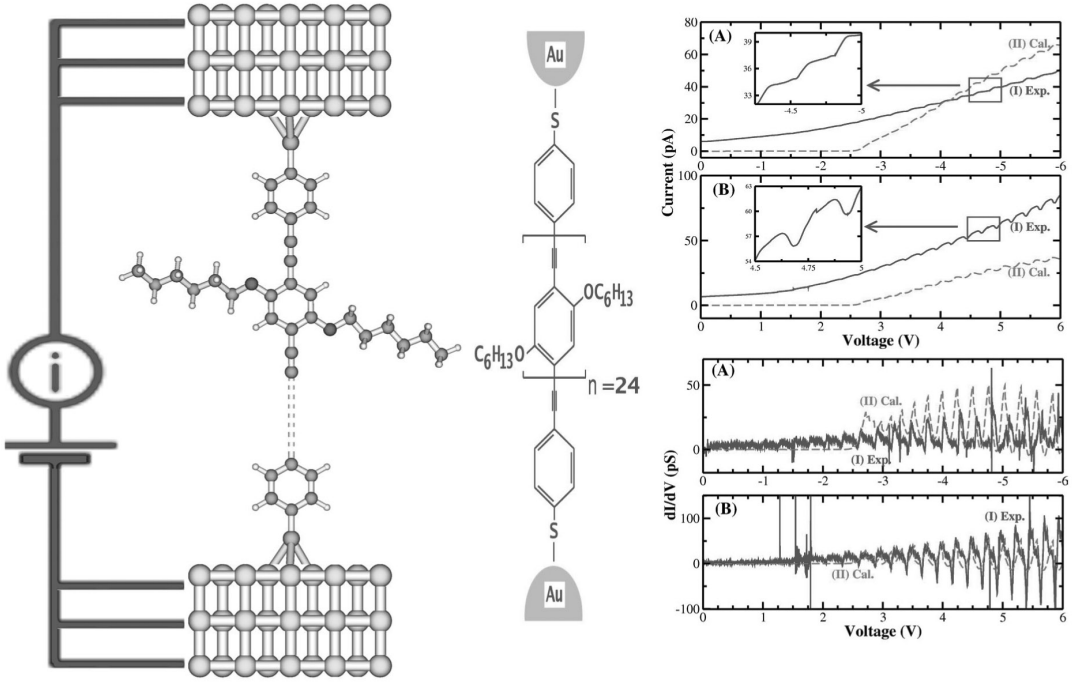

Fig. 25 (left) Connection model of TA-PPE between Au nanogap electrodes; (right) I-Vs of TA-PPE molecular junction and comparison of experimental (I, solid line) and theoretical (II, dashed lines) results.

The I-Vs of the polymer molecular junction were recorded at room temperature in a 1 Pa vacuum chamber. The current of pure nanogap electrodes (18 nm gap) has a noise level of several fA under the same conditions. Several features have been clearly identified in the I-V characteristics (Fig. 25): (i) highly periodic, identical, and repeatable stepwise behavior appears, which is more profound under a positive bias; (ii) the separation between the neighboring steps (or peaks) is always around 0.23–0.26 V; and (iii) the I-Vs are not symmetric with respect to the voltage inversion.

One possible explanation for the I-Vs could relate to the Coulomb charging effect [35], where each step (or peak) corresponds to the injection of one electron into the polymer molecule. Another possible mechanism for the stepwise behavior could relate to resonant electron tunneling: each step indicates the opening of a conducting channel that corresponds to the molecular orbitals of the polymer molecule [36].

First-principles calculation has been well applied to the transport properties of molecular devices (small molecules, e.g., benzene-1,4-dithiolate [37]) as well as alkanethiols [38]. Therefore, we carried out density functional theory (DFT) calculations for polymer molecules of different lengths to understand both the Coulomb charging and resonant tunneling mechanisms using the GAUSSIAN03 [39] program at the hybrid DFT B3LYP level with Lanl2dz (for Au) and 6-31G (for the rest) basis sets. A generalized quantum chemical Green's function approach [40] implemented in the QCME program [41] has been used to simulate the I-V characteristics of polymer molecular devices.

Based on the elastic scattering Green's function approach, we calculated current and conductance curves for the neutral polymer with 10 units (poly10), which show clearly repeatable stepwise behavior. In the simulations, we assumed that the potential drops largely at the interfaces, which is a reasonable approximation for a weakly bonded long chain system [42]. The energy separation between different peaks is 0.5 eV, which is exactly twice the orbital energy difference between different conducting channels of the poly10 molecule. The resonant electron tunneling mechanism seems to provide a straightforward explanation for the experimental results. The electrode gap in the experiment is around 18 nm, which corresponds to the length of TA-PPE polymer with 24 units (poly24). The calculated I-V characteristics of poly24 are shown in Fig. 25 together with the corresponding experimental results. The theoretical and experimental results are in good agreement. It is clear that the well-spaced molecular orbital in poly24 is responsible for the step-wise feature in the I-V curve. Different steps correspond to the opening of different conducting channels. The calculated voltage spacing between different steps of poly24 is around 0.26 V, which is in perfect agreement with the experimental value of 0.23–0.26 V. It is interesting to see that the electronic structure of an 18-nm-long TA-PPE polymer is still largely quantized.

SUMMARY AND FURTHER EXPERIMENTS

The above analysis shows that conjugated polymers with the characteristics of conductivity, rigidity, and connectivity can be employed for nanodevices. The combination of conjugated polymers (polymer electronics) and nanodevices (nanoelectronics) has generated a possible new research direction (Fig. 26): polymer nanoelectronics.

In terms of further research on polymer nanodevices it will be interesting (i) to determine the dependence of the transport properties of TA-PPE on the length of the polymer backbone, i.e., the average number of polymerization units n; (ii) to fabricate polymer nanocircuits with TA-PPE by self-assembly; and (iii) to adjust the transport properties of TA-PPE by changing its molecular structure. For example, it was found that the properties of oligomer phenylene ethynylene (OPE) could be changed when a redox center (e.g., $–NO_2$) was introduced into OPE [43], although the mechanism remains unclear [44].

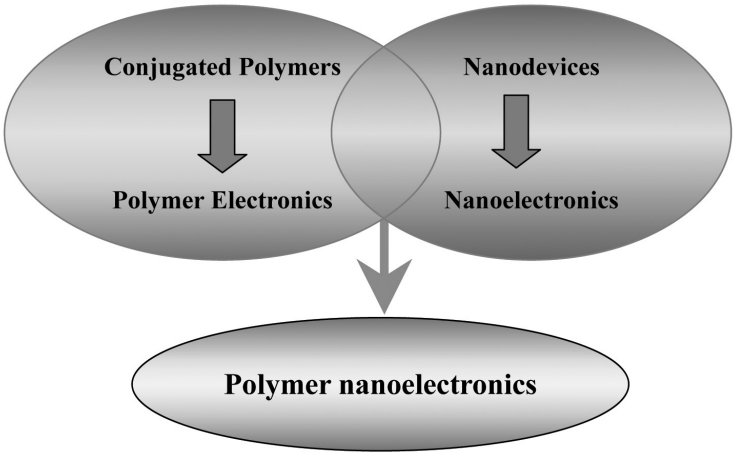

Fig. 26 Combination of polymer electronics and nanoelectronics for polymer nanoelectronics.

Tetrathiafulvalene (TTF) and its derivatives, which are good donors, are widely used in organic conductors and superconductors as well as materials chemistry [45]. The measured conductivity of a self-assembling monolayer of TTF derivatives on a Au(111) surface revealed the high conductivity of TTF molecules [46], which could constitute a good bridge for electron transfer [47]. Considering the unique properties of TTF, we reasoned that the introduction of a TTF unit into TA-PPE would greatly alter the properties of the polymer, and even change the conductive mechanism of the molecules from tunneling to thermal hopping because of the stability of the TTF radical (a long-lived radical might change the conductance mechanism [48] and the hopping mechanism requires that the carrier should actually reside on the wire [49]). More importantly, it can help us to clarify the relationship between the redox center and the properties of polymer molecules. Based on these considerations, we introduced a TTF unit into the TA-PPE backbone chain [50], and the molecular structure is shown in Fig. 27 (we call this TTF-TA-PPE).

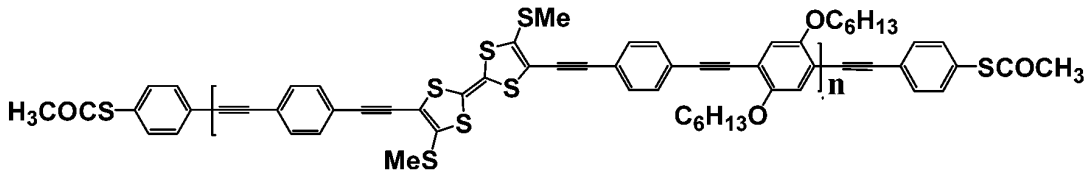

Fig. 27 Molecular structure of TTF-TA-PPE.

ACKNOWLEDGMENTS

The authors are grateful to Dr. Hideaki Takayanagi (Director, NTTBRL) and Dr. Hiroshi Inokawa (NTTBRL) for provocative discussions. W. H. and H. L. acknowledge support from the National Natural Science Foundation of China (20421101, 20404013, 20402015, 90401026, 20527001), the Ministry of Science and Technology and the Chinese Academy of Sciences. Y. L. acknowledges support from the Swedish Research Council and the Carl Trygger Foundation.

REFERENCES

1. J. H. Burroughes, D. D. C. Bradley, A. R. Brown, R. N. Marks, K. Mackay, R. H. Friend, P. L. Burns, A. B. Holmes. *Nature* **347**, 539 (1990).
2. K. Furukawa. *Acc. Chem. Res*. **36**, 102 (2003).
3. U. H. Bunz. *Chem. Rev.* **100**, 1605 (2000).
4. P. Samorí, N. Severin, K. Muellen, J. P. Rabe. *Adv. Mater.* **12**, 579 (2000).
5. J. M. Tour, L. Jones II, D. L. Pearson, J. J. S. Lamba, T. P. Burgin, G. M. Whitesides, D. L. Allara, A. N. Parikh, S. V. Atre. *J. Am. Chem. Soc*. **117**, 9529 (1995).
6. G. S. McCarty, P. S. Weiss. *Chem. Rev*. **99**, 1983 (1999).
7. P. Samori. *J. Mater. Chem*. **14**, 1353 (2004).
8. E. Tran, M. A. Rampi, G. Whitesides. *Angew. Chem., Int. Ed.* **43**, 3835 (2004).
9. A. Bezryadin, C. Dekker. *J. Vac. Sci. Technol. B* **15**, 793 (1997).
10. H. Park, A. K. L. Lim, A. P. Alivisatos, P. L. McEuen. *Appl. Phys. Lett.* **75**, 301 (1999).
11. A. F. Morpurgo, C. M. Marcus, D. B. Robinson. *Appl. Phys. Lett*. **74**, 2084 (1999).
12. X. D. Cui, A. Primak, X. Zarate, J. Tomfohr, O. F. Sankey, A. L. Moore, T. A. Moore, D. Gust, G. Harris, S. M. Lindsay. *Science* **294**, 571 (2001).
13. B. Q. Xu, N. J. Tao. *Science* **301**, 1221 (2003).
14. N. Chopra, W. T. Xu, L. De Long, B. J. Hinds. *Nanotechnol*. **16**, 133 (2005).
15. M. A. Reed, C. Zhou, C. J. Muller, T. P. Burgin, J. M. Tour. *Science* **278**, 252 (1997).
16. Q. Qing, F. Chen, P. Li, W. Tang, Z. Wu, Z. Liu. *Angew. Chem., Int. Ed.* **44**, 7771 (2005).
17. K. Liu, P. Avouris, J. Bucchignano, R. Martel, S. Sun, J. Michl. *Appl. Phys. Lett*. **80**, 865 (2002).
18. H. Park, A. K. L. Lim, A. P. Alivisatos, J. Park, P. L. McEuen. *Appl. Phys. Lett*. **75**, 301 (1999).
19. S. H. Liu, J. B. H. Tok, Z. Bao. *Nano Lett.* **5**, 1071 (2005).
20. H. Nakashima, K. Furukawa, Y. Kashimura, K. Torimitsu. *Polymer Preprints* **44**, 482 (2003).
21. K. Furukawa, H. Nakashima, K. Ajoto, Y. Kashimura, W. Hu, K. Torimitsu. *Jpn. J. Appl. Phys.* **43**, 4521 (2004).
22. W. Hu, H. Nakashima, K. Furukawa, Y. Kashimura, K. Ajito, K. Torimitsu. *Appl. Phys. Lett*. **85**, 115 (2004).
23. P. Kohli, K. K. Taylor, J. J. Harris, G. J. Blanchard. *J. Am. Chem. Soc.* **120**, 11962 (1998).
24. H. Nakashima, K. Furukawa, K. Ajito, Y. Kashimura, K. Torimitsu. *Langmuir* **21**, 511 (2005).
25. W. Hu, H. Nakashima, K. Furukawa, Y. Kashimura, K. Ajito, K. Torimitsu. *Appl. Phys. Lett*. **85**, 115 (2004).
26. B. J. van Wees, H. van Houten, C. W. J. Beenakker, J. G. Williamson, L. P. Kouwenhoven, D. van der Marel, C. T. Foxon. *Phys. Rev. Lett*. **60**, 848 (1988).
27. D. H. Waldeck, D. N. Beratan. *Science* **261**, 576 (1993).
28. W. Hu, H. Nakashima, K. Furukawa, Y. Kashimura, K. Ajito, C. Han, K. Torimitsu. *Phys. Rev. B* **69**, 165207 (2004).
29. M. di Ventra, S. T. Pantelides, N. D. Lang. *Phys. Rev. Lett*. **84**, 979 (2000).
30. J. G. Kushemerick, D. B. Holt, J. C. Yang, J. Naciri, M. H. Moore, R. Shashidhar. *Phys. Rev. Lett.* **89**, 086802 (2002).
31. S. M. Sze. *Physics of Semiconductor Devices*, 2nd ed., Chap. 7, John Wiley, New York (1981).
32. W. Wang, T. Lee, M. A. Reed. *Phys. Rev. B* **68**, 035416 (2003).
33. W. Hu, H. Nakashima, K. Furukawa, Y. Kashimura, K. Ajito, Y. Liu, D. Zhu, K. Torimitsu. *J. Am. Chem. Soc.* **127**, 2804 (2005).
34. W. Hu, J. Jiang, H. Nakashima, Y. Luo, Y. Kashimura. K. Chen, Z. Shuai, K. Furukawa, W. Lu, Y. Liu, D. Zhu, K. Torimitsu. *Phys. Rev. Lett.* **96**, 027801 (2006).
35. S. Kubatkin, A. Danilov, M. Hjort, J. Cornil, J. L. Bredas, N. Stuhr-Hansen, P. Hedegard, T. Bjornholm. *Nature* **425**, 698 (2003).
36. A. Javey, J. Guo, Q. Wang, M. Lundstrom, H. Dai. *Nature* **424**, 654 (2003).

37. M. Di Ventra, S. T. Pantelides, N. D. Lang. *Phys. Rev. Lett.* **84**, 979 (2000).
38. Y. C. Chen, M. Zwolak, M. Di Ventra. *Nano Lett.* **5**, 621 (2005).
39. Gaussian 03, Revision A.1, M. J. Frisch et al. Gaussian, Inc., Pittsburgh PA (2003).
40. J. Jiang, W. Lu, Y. Luo. *Chem. Phys. Lett.* **400**, 336 (2004).
41. Jun Jiang, Yi Luo. QCME-V1.0-Quantum Chemistry for Molecular Electronics.
42. Y. Gohda, S. T. Pantelides. *Nano Lett.* **5**, 1217 (2005).
43. F. R. Fan, R. Lai, J. Cornil, Y. Karzazi, J. Brédas, L. Cai, L. Cheng, Y. Yao, D. Price, S. Dirk, J. M. Tour, A. J. Bard. *J. Am. Chem. Soc.* **126**, 2568 (2004).
44. X. Xiao, L. A. Nagahara, A. M. Rawlett, N. Tao. *J. Am. Chem. Soc.* **127**, 9235 (2005).
45. J. L. Segura, N. Martin. *Angew. Chem., Int. Ed.* **40**, 1372 (2001).
46. E. Gomar-Nadal, G. Ramachandran, F. Chen, T. Burgin, C. Rovira, D. Amabilino, S. Lindsay. *J. Phys. Chem. B* **108**, 7213 (2004).
47. N. Gautier, F. Dumur, V. Lloveras, J. Vidal-Gancedo, J. Veciana, C. Rovira, P. Hudhomme. *Angew. Chem., Int. Ed.* **42**, 2765 (2003).
48. F. Maya, S. Chanteau, L. Cheng, M. Stewart, J. M. Tour. *Chem. Mater.* **17**, 1331 (2005).
49. D. Adams, L. Brus, C. Chidsey, S. Creager, C. Creutz, C. Kagan, P. Kamat, M. Lieberman, S. Lindsay, R. Marcus, R. Metzger, M. Michel-Beyerle, J. Miller, M. Newton, D. Rolison, O. Sankey, K. Schanze, J. Yardley, X. Zhu. *J. Phys. Chem. B* **107**, 6668 (2003).
50. E. Wang, H. Li, W. Hu, D. Zhu. *J. Polym. Sci., Part A: Polym. Chem.* **44**, 2707 (2006).